Microporous and Mesoporous Materials 235 (2016) 59–68

Contents lists available at ScienceDirect

Microporous and Mesoporous Materials

journal homepage: www.elsevier.com/locate/micromeso

Protein encapsulation in SBA-15 with expanded pores

P.R.A.F. Garcia [a], R.N. Bicev [b], C.L.P. Oliveira [b], O.A. Sant'Anna [c], M.C.A. Fantini [a, *]

[a] Instituto de Física da Universidade de São Paulo, Departamento de Física Aplicada, Rua do Matão, 1371, Cidade Universitária, 05508-090, São Paulo, SP, Brazil
[b] Instituto de Física da Universidade de São Paulo, Departamento de Física Experimental, Rua do Matão, 1371, Cidade Universitária, 05508-090, São Paulo, SP, Brazil
[c] Instituto Butantan, Laboratório de Imunoquímica, Avenida Vital Brasil, 1500, 05503-900, São Paulo, SP, Brazil

ARTICLE INFO

Article history:
Received 14 April 2016
Received in revised form
5 July 2016
Accepted 24 July 2016
Available online 26 July 2016

Keywords:
SBA-15
SAXS
BSA
HGG

ABSTRACT

This work reports the encapsulation of proteins with different molecular weights into SBA-15 ordered mesoporous silica, a potential immunological adjuvant. The Human Gammaglobulin G (HGG) and Bovine Serum Albumin (BSA) proteins were incorporated into the mesoporous silica with expanded pores. A structure swelling agent, triisopropylbenzene (TIPB), was used in the synthesis process, promoting an increase of the average pore diameter and a more disordered pore network, as revealed by nitrogen adsorption isotherm (NAI) and small angle X-ray scattering (SAXS) data. SAXS measurements were also performed to obtain the overall size of the studied proteins. The results showed that both proteins have dimensions that would allow their encapsulation inside the pores of SBA-15. The HGG and BSA proteins were dissolved in phosphate buffered saline (PBS) solutions before encapsulation. It was evidenced the filling of the micropores by the PBS solution and a larger variation in pore volume and surface area for the material with higher mean pore diameter, which was also confirmed by the modeling of SAXS data. It was not observed any significant difference in the SAXS and NAI results of both proteins, indicating that the immunogens could be encapsulated in the silica macroporosity, obstructing the mesopore entrances.

1. Introduction

Materials with adjustable porous structure have always been of great interest for industry and academic community. Their advantageous properties are a narrow distribution of pore sizes, large surface areas and pore volumes. Microporous aluminosilicates with pore diameters less than 2 nm, known as zeolites, often satisfy these conditions and thus find many applications in catalysis and molecule selection. However, the use of zeolites is restricted to the size of their pores. In the last decades there was a growing demand for ordered mesoporous materials due to their potential application on the encapsulation of large molecules [1].

The family M41S of ordered mesoporous materials (OMM) was developed by Mobil Corporation Laboratories in the early 90s and the first developed silica structure was MCM-41, whose average pore diameter is 4 nm [2]. This material consists of pores arranged in a hexagonal symmetry with amorphous silica walls. According to the definition of the International Union of Pure and Applied Chemistry (IUPAC) [3], the so called "mesoporous materials" should display pore diameters between 2 and 50 nm.

Since the discovery of OMM, the use of surfactants as structure-directing agents and the development of synthesis routes and conditions in which an ordered structure is formed were explored in a large number of publications in the literature. Nonionic polymer surfactants also started to be used. Pinnavaia et al. [4] developed worm-like disordered mesoporous silica with pore sizes between 2 and 5.8 nm using nonionic surfactants in a neutral aqueous medium.

Using nonionic surfactants of high molecular weight in acidic aqueous medium (pH ~ 2), Zhao et al. [5] obtained highly ordered mesoporous silica (OMS), named SBA-15. In the synthesis of this silica, the associations between silicate species and polymer occur through hydrogen bonds [6]. Examples of OMS obtained with neutral surfactants are the SBA-11 (cubic), SBA-12 (hexagonal) and SBA-14 (cubic).

The main route of synthesis of these materials utilizes three basic reagents: a structure-directing agent, a solvent and a silicon

* Corresponding author.
E-mail address: mfantini@if.usp.br (M.C.A. Fantini).

http://dx.doi.org/10.1016/j.micromeso.2016.07.033
1387-1811/

source; the construction comprises an activated self-assembly process, leading to the formation of polymeric micelles by a mechanism known as Liquid Crystal Template (LCT), proposed by Kresge and Beck [2,7].

OMSs have applications in several areas such as petroleum refining industry, catalysis and microelectronics [8–10]. The capacity to release and adsorb molecules inside the pores of these materials has been extensively studied also for medical applications [11–13]. For example, the encapsulation of drugs such as anti-inflammatory ibuprofen [14], camptothecin and immobilization of globular enzymes [15] has been carried out.

A major advantage of using copolymers as structure-directing agents is the possibility of adjusting the pore diameter by changing the size of the polymer chains. Another possibility is the expansion of the micelles by the use of swelling agents such as 1,3,5-trimethylbenzene (TMB) and 1,3,5-triisopropylbenzene (TIPB). When these agents are added in the synthesis, they are solubilized with the hydrophobic portion of the micelle. In particular, this approach is preferable since the pore size could, in principle, be increased continuously by increasing the amount of the swelling agent [16].

In the field of immunology, the pioneer studies of Mercuri et al. [17] and Carvalho et al. [18] demonstrated that the SBA-15 acts as an efficient adjuvant. These studies showed unusual antibody production when the isogenic BALB/c line and the genetically selected High or Low outbred antibody responders mice were immunized with the SBA-15 as a vehicle to transport antigens. The tested antibody responses were performed with 16.5 kDa *Escherichia coli* recombinant protein Intimin 1β, *Micrucurus ibiboboca* snake venom proteins with molecular weights ranging from 7 to 8 kDa and 66 kDa bovine serum albumin (BSA). The SBA-15 promoted similar or higher responses than the aluminum hydroxide and Incomplete Freund's adjuvants.

Another advantage of the use of the non-toxic SBA-15 is that it does not cause any tissue damage in the application area of injection and, therefore, does not produce unwanted effects presented by other adjuvants [17]. The BSA release from SBA-15 in gastric and intestinal fluids was also explored, as well the presence of silicon in mice organs, showing its applicability as an oral vaccine adjuvant [19]. Moreover, SBA-15 protects the antigens from hostile stomach environment and proteases, providing the efficacious catabolic activity of antigen presenting cells (APC), such as macrophages and dendritic cells, thereby allowing an effective immunogenicity [17].

For these applications, the knowledge about protein encapsulation process is fundamental. Information on the filling of surface area and pore volume are very important to determine optimal conditions for the system such as the appropriate protein:silica concentration and suitable pore size, among others.

Here, the incorporation of proteins in SBA-15 samples with expanded pores was investigated by small angle X-ray scattering (SAXS) and nitrogen adsorption isotherms (NAI). The efficiency of incorporation of the Human Gammaglobulin G (HGG) and bovine serum albumin (BSA) was compared. In order to promote the expansion of the pores, TIPB was added to the silica synthesis. SAXS measurements provided information about the porous network and also an estimation of the protein dimensions. This information is necessary in order to verify the possibility of encapsulation inside the silica pores. An advanced theoretical model was applied to analyze the SAXS data permitting the retrieval of valuable structural information. The NAI measurements were used for textural information such as pore volume, surface area and pore diameter.

2. Materials and methods

2.1. Synthesis of SBA-15 samples

Three samples of SBA-15 with different amounts of the TIPB swelling agent were prepared. They are: P0, P05 and P2, where the number indicates the mass ratio TIPB/P123 (the sample P0 has a mass ratio TIPB/P123 = 0 and therefore it is a conventional sample SBA-15). The synthesis route for conventional SBA-15 was used [20], but with the addition of TIPB in the formulation. The TIPB/P123 ratios were chosen to check the effect on the OMS morphology of a small (TIPB/P123 = 0.5) and large (TIPB/P123 = 2.0) amount of TIPB.

For the synthesis of these samples, 1 g of the triblock copolymer Pluronic P123 ($PEO_{20}PPO_{70}PEO_{20}$), from BASF, was solubilized with 30.5 g of hydrochloric acid at a concentration of 2 mol L^{-1}. The solution was kept under magnetic stirring for two hours at 40 °C. Then 2.15 g of the silicon source, tetraethyl orthosilicate, TEOS (from Fluka), and the swelling agent TIPB (from Sigma-Aldrich) were added to the solution and the mixture was kept under magnetic stirring for more 24 h. The resulting solution was inserted in an autoclave and submitted to hydrothermal treatment at 100 °C for 48 h. After, the sample was washed with deionized water and dried at 100 °C for 24 h. The resulting material was calcined at 540 °C for two hours under nitrogen atmosphere and for 4 h in air in order to remove the polymer.

The incorporation of BSA (66.5 kDa, from Sigma-Aldrich) and HGG (150 kDa, from Sigma-Aldrich) was performed by dissolving these proteins and the silica samples in a phosphate-buffered saline solution (PBS). The mass proportion protein:silica used was 1:5. For the incorporation, 20 mg of the protein were dissolved in 10 ml of PBS and kept under magnetic stirring for 45 min. Then, 100 mg of silica were added and the solution was stirred for 30 min. After that, the samples were dried at 35 °C for 96 h. Table 1 identifies the samples studied in this work.

The samples with BSA were named P0B, P05B and P2B. The samples with HGG were named P0H, P05H and P2H. One conventional SBA-15 sample was prepared with only PBS and was named P0P.

2.2. SAXS experimental conditions and analysis

The samples P2, P2B, P2H and the proteins were characterized in experiments performed in a small angle X-ray scattering camera (Xenocs, Xeuss), placed at the Institute of Physics, University of São Paulo. The set-up has a microfocus Genix X-ray source (CuKα radiation), focusing X-ray mirrors, two scatterless slits sets and a Pilatus two-dimensional detector.

All other SBA-15 samples were characterized on a Bruker AXS Nanostar small angle X-ray scattering camera also placed at the Institute of Physics, University of São Paulo. This camera has a microfocus Genix 3D system (source + focusing mirrors), two scaterless slits sets for collimation and a 2D Vantec-2000 detector.

For both cameras the X-ray wavelength was λ = 1.5418 Å, the cross section of the beam was 0.8 × 0.8 mm^2 and sample to detector distance were 66.7 cm for the Nanostar and 72.5 cm for the Xeuss.

Table 1
SBA-15 samples with proteins and different amounts of TIPB. In addition to the samples shown in this table there is also the sample with PBS, named P0P.

SAMPLE	P0	P0B	P0H	P05	P05B	P05H	P2	P2B	P2H
TIPB/P123	0	0	0	0.5	0.5	0.5	2	2	2
PROTEIN	–	BSA	HGG	–	BSA	HGG	–	BSA	HGG

The range of scattering vectors q ($q = (4\pi/\lambda)\sin\theta$, where 2θ is the scattering angle) was 0.01 $Å^{-1}$ to 0.35 $Å^{-1}$.

SBA-15 samples, in powder form, were placed between two mica sheets and the measurements were performed at room temperature for exposure times of 600 s.

The protein samples were prepared in PBS solution at a concentration of 3 g L^{-1}. They were stored on sealed quartz capillaries, which were glued on stainless steel cases. The capillaries were rinsed and reused, enabling a reliable background subtraction. The exposure times were 1800 s and around 30 frames were obtained for each protein. This large number of frames was useful to investigate the stability of the proteins over time. The SAXS measurement of HGG was performed at a temperature of 38 °C because the protein is more stable at this temperature. Measurements of the BSA sample were performed at room temperature (T ~ 20 °C).

The SAXS data measured with the Vantec-2000 detector were corrected for detector efficiency and spatial distortions. The azimuthal average was calculated for the whole q range. The scattering of the two mica foil was used as background and it was subtracted from the sample data. For the proteins the PBS scattering was used as background. All the data treatment was performed by using the program SUPERSAXS (Oliveira and Pedersen, unpublished).

SAXS measurements of the protein samples were converted to absolute scale so that the unit of the scattering intensity I(q) is cm^{-1}. Since there was no need to express the SAXS data of the samples of SBA-15 in absolute scale, these data were shown in arbitrary units.

The lattice parameter a is a function of diffraction peak positions and for hexagonal structures it is given by:

$$\left(\frac{q_{hkl}}{2\pi}\right)^2 = \frac{4}{3}\left(\frac{h^2 + hk + k^2}{a^2}\right) + \frac{l^2}{c^2} \quad (1)$$

where h, k and l are Miller indices; q_{hkl} is the central value of the diffraction peak with the (hkl) index. SBA-15 pores network is a 2D hexagonal system, so that $l = c = 0$. Equation (1) was applied to the peaks (100) of the SAXS curves to calculate the lattice parameter of the samples. A Gaussian curve was fitted to these diffraction peaks to determine their central value (q_{hkl}).

Estimations of the size of the proteins was performed using the pair-distance distribution p(r) evaluated through the Indirect Fourier Transform (IFT) method. The function p(r) is the Fourier transform of the scattering intensity I(q). By the use of the IFT method the scattering intensity I(q) may be obtained through the function p(r) by Ref. [21]:

$$I(q) = 4\pi \int_0^{D_{max}} \frac{p(r)\sin(qr)}{qr} \quad (2)$$

where D_{max} is the largest dimension of a particle. The integral is calculated from 0 to D_{max} because the p(r) function vanishes for $r > D_{max}$ and $r = 0$.

In the IFT method the function p(r) is described by a series of orthogonal functions, and the indirect Fourier transform (Equation (2)) is calculated to obtain the function in reciprocal space, seeking the curve which best describes the experimental I(q) data. This process was performed by the Gnom software [22].

The function p(r) can be used to determine the maximum particle diameter D_{max} and it also provides information on the particle shape [23].

Since the atomic resolution model for the BSA protein is known, it is possible to compare the experimental SAXS data with the theoretical scattering intensity obtained from this model. The file with the atomic coordinates (PDB file) was obtained at the protein data bank website (id code: 4F5S). Interestingly, the asymmetric unit on the pdb file is a dimer and therefore is possible to describe the SAXS data either with a monomer or with dimers of BSA. The fits were performed by the use of the program Crysol [24].

For the proper description of the BSA SAXS data, it was necessary to assume a polydisperse system composed of monomers and dimers in the system. Therefore it was possible to determine the volume fractions of monomers and dimers of the BSA sample using the software Oligomer [25]. This software uses the theoretical scattering curves obtained from atomic coordinates (program Crysol), providing the volume fractions of each species that give the best fit of the experimental data. The scattering intensity of a sample that is composed of K components is written as:

$$I(q) = \sum_{i=1}^{K} (w_i \times I_i) \quad (3)$$

where w_i and I_i are the volume fraction and the scattering intensity of the i-th component, respectively.

In order to obtain additional information on experimental SAXS data for the samples with ordered mesopores, a theoretical model including geometrical considerations can be used [26]. In this work it was applied an advanced model procedure, described by Manet et al. [27] and Sundblom et al. [28], developed to describe hexagonal ordered mesoporous silicas. The final theoretical intensity is decomposed into the form factor and the structure factor contributions, permitting a full curve fitting. It is based on a system of core-shell cylinders, with a diffuse outer interface. Here, the cylinders core can be understood as the pores of the SBA-15 and the overall scattering intensity can be expressed by:

$$I(q) = (\rho_1 - \rho_2)^2 nP(q)\cdot S(q) + I(q)_{chain} \quad (4)$$

where $(\rho_1 - \rho_2)$ is the electron density contrast between the pores and the silica matrix, n is the number of pores per unit volume, $P(q)$ is the form factor, $S(q)$ is the structure factor and $I(q)_{chain}$ is the scattering intensity of micropores. This intensity due to the micropores is given by the Debye formula for Gaussian chains [29]:

$$I_{chain}(q) = \frac{2\left[e^{-q^2R_g^2} - 1 + \left(q^2R_g^2\right)\right]}{\left(q^2R_g\right)^2} \quad (5)$$

In equation (5) R_g is the average radius of gyration of the chains.

As the length of the pores of SBA-15 is very large compared to its diameter one can use the decoupling approximation [30]. The form factor can be expressed as the form factor of an infinitely long rod (P_{rod}) [31] times the form factor of the cross-section of a cylinder (P_{CS}):

$$P(q) = P_{rod}(q)\cdot P_{CS}(q) \quad (6)$$

where $P_{CS}(q)$ is given by:

$$P_{CS}(q) = \left(\frac{2J_1(qR)}{qR}\right)^2 \quad (7)$$

where $J_1(qR)$ is a Bessel function.

A scale factor Sc_{const} was added to describe the background. The final expression of this model is:

$$I(q) = Sc_1 P_{rod}\left\langle F_{CS}^2(q)\right\rangle(1+\beta(q)[\langle Z(q)\rangle - 1]G(q)) + Sc_2 I(q)_{chain} + Sc_{const} \quad (8)$$

where Sc_1 is the scale factor of the mesopores, F_{CS} is the cross-sectional amplitude of the mesopores, $Z(q)$ is the lattice factor describing the spatial distribution of the mesopores, Sc_2 is scale factor of the micropores and $I(q)_{chain}$ is the scattering intensity due to micropores. The $\beta(q)$ factor is related to the polydispersity in pore diameter. A nonlinear least-square method was used to fit the curve given by Equation (8) to the experimental data.

The scattering intensity is affected by the smearing effects, which are caused by the finite size of the beam and finite resolution of the detector. To take this effect into account, the experimental intensity $\widetilde{I}(q)$ is calculated considering a resolution function $R(<\boldsymbol{q}>,q)$ [32]:

$$\widetilde{I}(q) = \int R(<\boldsymbol{q}>,q)I(q)dq \quad (9)$$

The parameters that comprise the model are shown in Table 2.

2.3. NAI experimental conditions

Nitrogen adsorption isotherms measurements were performed using Micromeritics ASAP 2020 equipment, placed at the Institute of Physics, University of São Paulo. This equipment has two degas stations and one analysis station. The samples were degassed for 24 h. The SBA-15 samples without protein were degassed at 200 °C, while the samples with protein were degassed at 40 °C to prevent the degradation of the proteins. The measurements were performed in a liquid nitrogen bath with relative pressures ranging from 10^{-6} to 0.995.

The pore surface area was determined by the BET method [33], the total pore volume and the pore size distribution (PSD) were determined by the BJH-KJS method [34,35] using the adsorption branch. The volume and surface area of micropores were determined by the t-plot method [36].

3. Results

3.1. The addition of TIPB

The SAXS data show that the addition of TIPB resulted in larger pores and a more disordered pore structure, as observed in other studies [16]. This fact is evidenced by the decrease in the integrated intensity of the diffraction peaks and the absence of (210) and (300) peaks in the curves of the samples with TIPB (Fig. 1). The (100) peaks are displaced to lower q values and this fact is related to the increase of the lattice parameters of these samples.

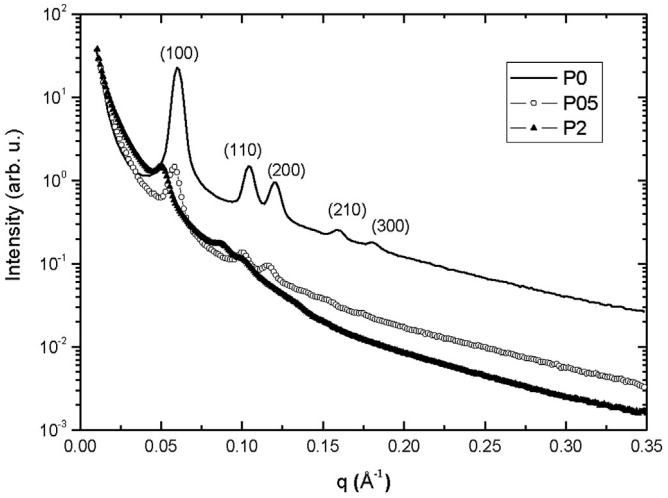

Fig. 1. SAXS curves of the conventional and pores expanded SBA-15 samples.

Table 3
Ratios between diffraction peak positions in reciprocal space of the silica samples and the expected value for a hexagonal lattice.

	$q_{(110)}/q_{(100)}$	$q_{(200)}/q_{(100)}$	$q_{(210)}/q_{(100)}$	$q_{(300)}/q_{(100)}$
P0	1.734	1.995	2.646	2.998
P05	1.727	1.992	–	–
P2	1.741	2.020	–	–
Expected value	1.732	2.000	2.646	3.000

If the pore network is ordered the positions of the diffraction peaks in reciprocal space will have well-defined ratios. In the case of the hexagonal network the ratios between the values of q of all peaks and the $q_{(100)}$ value of the (100) peak are $\sqrt{1}$, $\sqrt{3}$, $\sqrt{4}$, $\sqrt{7}$ and $\sqrt{9}$ [37]. Table 3 shows the calculated value of these ratios for all samples. These values are very close to those expected for a hexagonal lattice.

The isotherms and the pore size distribution are presented in Fig. 2. The NAI data, shown in Table 4, reveal that the TIPB addition caused a decrease of the BET specific surface areas. The BET specific surface areas of the samples with expanded pores

Table 2
Parameters included in the theoretical SAXS model.

Sc_1	Scale factor of the contribution of the mesopores
Sc_2	Scale factor of the contribution of the micropores
Sc_{const}	Background scale factor
c	Correction constant for conservation of the Porod invariant
a	Lattice parameter
D	Domain size
ν	Peak shape parameter
σ_a	Disorder parameter
R_{in}	Inner radius of the cylinder
R_{out}	Outer radius of the cylinder
L	Length of the cylinder
$\Delta\rho_{out}/\Delta\rho_{in}$	Ratio between outer and inner electron density contrast of the cylinder
σ_{in}	Length of the Gaussian interface
σ_R/R	Relative polydispersity
Rg	Average radius of gyration of the micropores

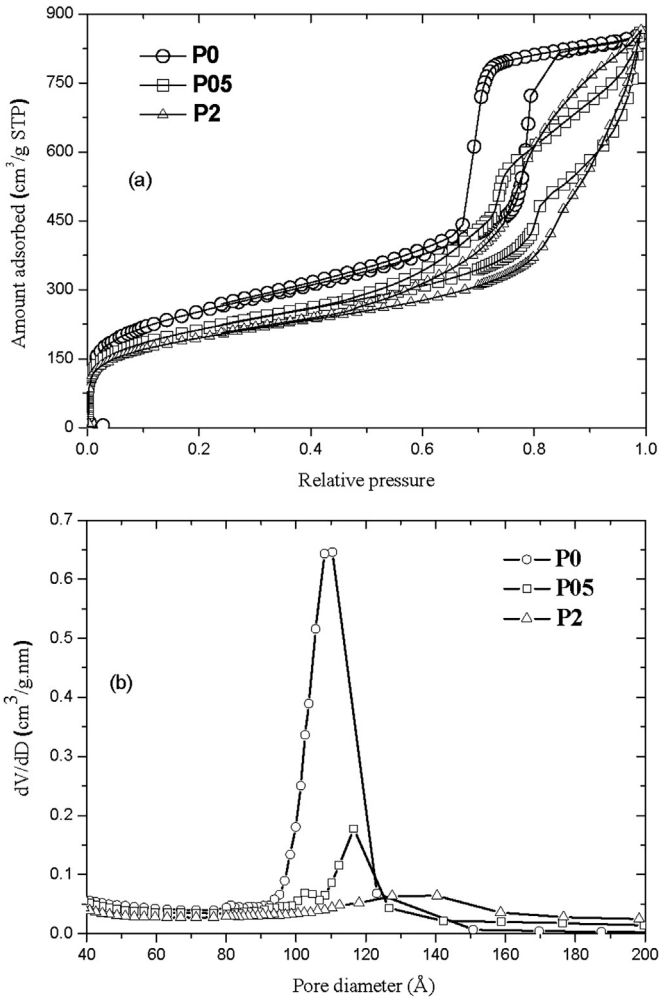

Fig. 2. (**a**) Isotherms and (**b**) pore size distribution of conventional and expanded pore SBA-15 samples.

presented reductions of 16% and 23%. The decrease in BET specific surface area is due to the cylindrical shape of the mesopores: since the specific total pore volume remained unchanged, an increase in the average pore diameter causes a decrease in the pore surface area [20].

The isotherm of P05 sample indicates a secondary porosity. This secondary porosity is also evident in the bi-modal pore size distribution curve of this sample which shows a small peak located at $D \approx 104$ Å. This result shows that the amount of TIPB was not enough to expand all pores of the matrix. On the other hand, the increase of TIPB mass during the synthesis to a larger TIPB/P123 ratio promoted an increase in lattice parameter, preserving the hexagonal structure, but with smaller ordered domains.

Table 4
NAI and SAXS data. Here V_t is the total pore volume, V_m is the micropore volume, A_{BET} is BET specific surface area, A_m is the micropore specific surface area, D_p is the average pore diameter and *a* is the lattice parameter. Errors in the fitting calculations of the BET area and the lattice parameter are less or equal to 0.5%.

	V_t (cm^3/g)	V_m (cm^3/g).10^{-2}	A_{BET} (m^2/g)	A_m (m^2/g)	D_p (Å)	a (Å)
P0	1.33	12.99 (25)	910	297 (4)	109	121
P05	1.33	13.80 (25)	765	304 (5)	117	125
P2	1.34	13.74 (22)	698	303 (4)	135	146

3.2. The characterization of the proteins

In order to estimate the dimensions of the proteins used in this work, SAXS measurements of the BSA and HGG diluted in PBS solution were performed.

First, the Gnom software was used to fit the experimental data SAXS of the BSA in solution, considering it as a monodisperse system [supplementary figures S1 (a) and (b)]. The maximum diameter of the particle provided by the fitting procedure was $D_{max} = 142$ Å, which is similar to the mean pore size of P2 sample. This maximum dimension is larger than the expected size for the native BSA (~90 Å). It is possible to show that the BSA sample is a polydisperse system composed of monomers and dimers, since the BSA atomic structure is known. One can compare the experimental scattering data with the theoretical calculated intensity. This can be performed by the use of the software Crysol. Interestingly, the asymmetric unit in the *pdb* file of the BSA is a dimer. Neither the monomers nor the dimers single models are capable to describe the SAXS data. Therefore, a mixture of monomers and dimers was calculated, using the software Oligomer. The form factors calculated by the program Crysol were used as input and the software optimized the volume fractions, as shown in equation (3). Fig. 3 shows the results, considering BSA as a monodisperse system of monomers, a monodisperse system of dimers and a polydisperse system of monomers and dimers, demonstrating a good agreement between experimental and model results of this last approach. Using this fit it was possible to determine the molecular mass through the gyration radius and the concentration of monomers and dimers. The background was also adjusted by adding a constant for all fits. Also, the *pdb* file was used in Massha software [38] to estimate the BSA dimensions. These data are shown in Table 5.

The maximum diameter obtained by the *p(r)* curve of BSA sample using the Gnom software agrees with the larger dimension of the dimer (140 Å) determined by Massha software. Also, the *p(r)* of BSA is characteristic of elongated particles and the peak at $r \approx 35$ Å corresponds to the average value of the other two dimensions (cross section dimensions) of the monomer and dimer, which are approximately 30 Å and 40 Å.

Fig. 4(a) and (b) show the SAXS curves of the HGG solution using Gnom software fit. The IFT modeling provides a good fitting of the SAXS curve and the overall dimensions obtained from the *p(r)*

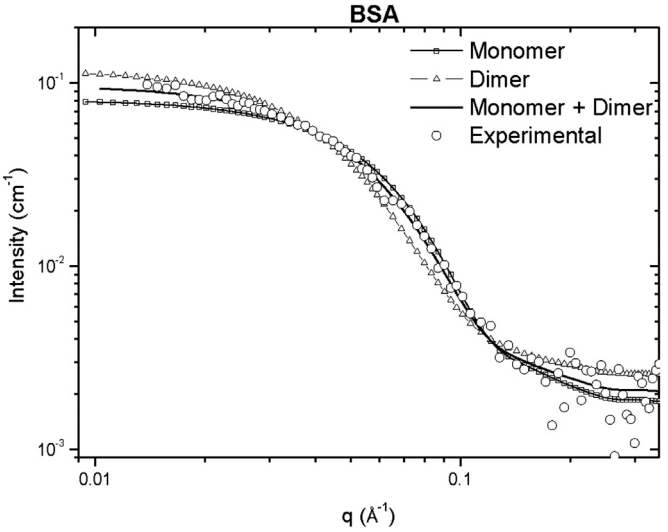

Fig. 3. BSA SAXS data, simulated as a monodisperse system of monomers, monodisperse system of dimers and polydisperse system of monomers and dimers.

Table 5
Molecular mass, volume fraction and dimensions of BSA particles.

	Monomers	Dimers
Molecular mass (kDa)	66.4	133.0
Volume fraction (%)	66.3 (4)	33.7 (3)
Dimensions (Å)	28 × 70 × 41	30 × 140 × 40

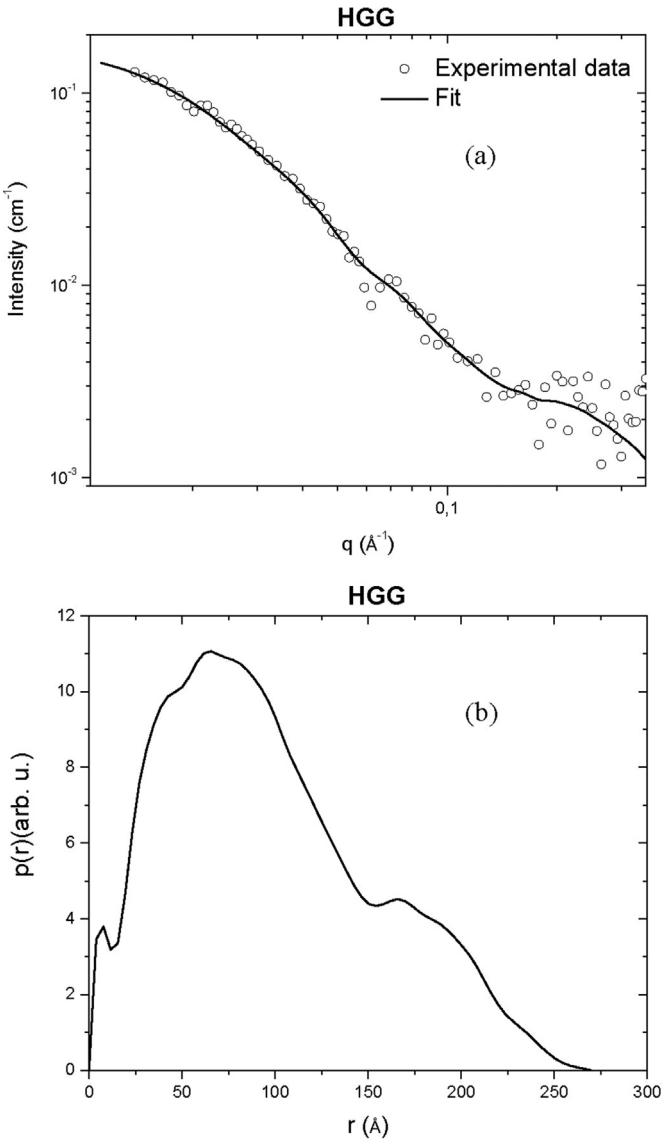

Fig. 4. (**a**) SAXS data fitting and (**b**) pair-distance distribution function for HGG samples.

curve of the HGG in solution was ~270 Å. This *p(r)* resembles the one obtained from elongated particles [39]. The obtained maximum size indicates that the protein is probably forming aggregates [40].

Other important aspect that may influence the incorporation is the particle flexibility. Information about flexibility can be obtained by the so called Kratky Plots ($I \times q^2$ *vs.* q). These plots indicated that the BSA protein is globular and compact, whereas the HGG protein presents higher degree of flexibility [supplementary information S2].

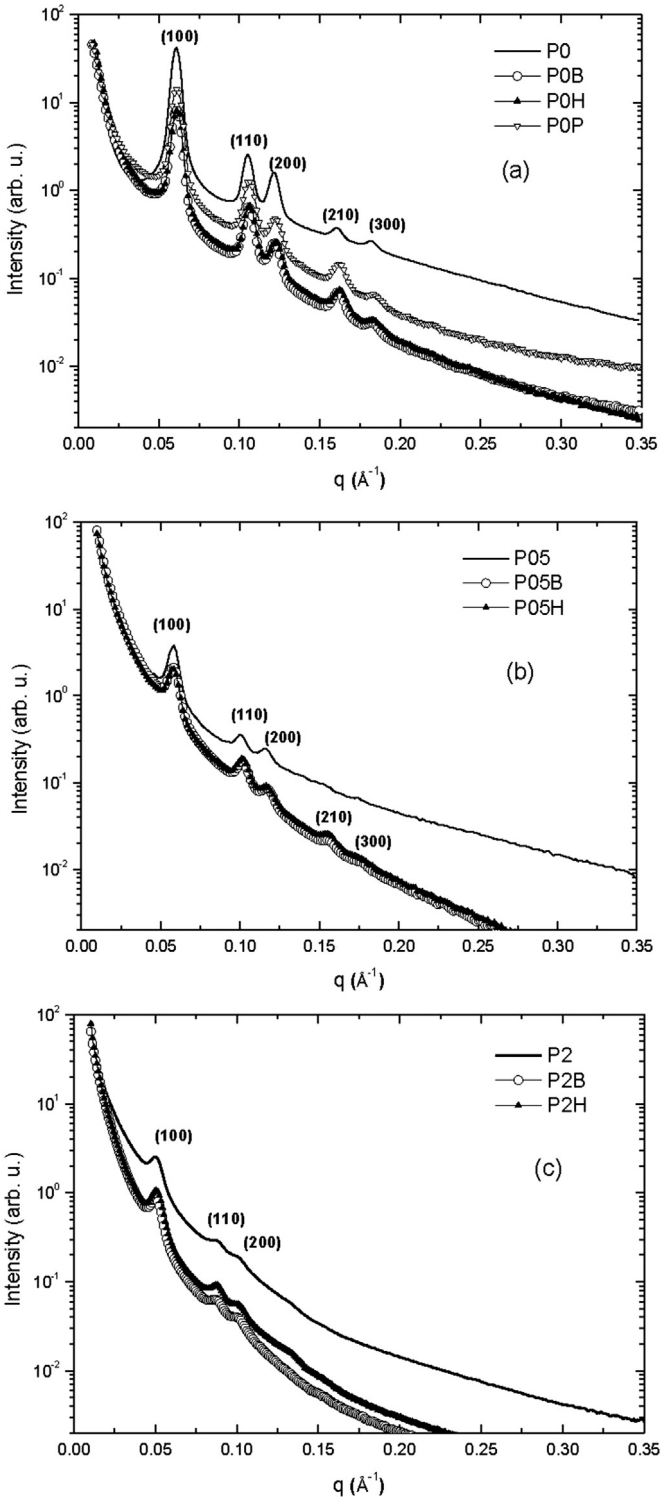

Fig. 5. SAXS curves of the (**a**) P0, (**b**) P05 and (**c**) P2 SBA-15 samples with proteins and PBS.

3.3. Incorporations of the proteins

The intensity of the SAXS curves of the SBA-15 samples with proteins (Fig. 5(a)-5(c)) is shifted to lower values. This is related to the absorption of the proteins present in the sample and also to the filling of the micropores by the PBS solution. The lattice parameter

Table 6
NAI and SAXS data of the silica samples with proteins. Here V_t is the total specific pore volume, V_m is the micropore specific volume, A_{BET} is the BET specific surface area, A_m is micropore specific surface area, D_P is the average pore diameter, a is the lattice parameter and A_{peaks} is the sum of the integrated areas of the (100), (110) and (200) diffraction peaks.

	V_t (cm^3/g)	V_m (cm^3/g)·10^{-2}	A_{BET} (m^2/g)	A_m (m^2/g)	D_P (Å)	a (Å)	A_{peaks} (arb. u.)
P0	1.33	12.99 (25)	910	297 (4)	109	121	269.35 (8)
P0B	0.58	0.34 (7)	256	15 (2)	107	121	52.20 (30)
P0H	0.57	0.33 (5)	208	14 (1)	108	120	52.82 (36)
P0P	0.44	0.33 (7)	188	14 (1)	111	120	103.51 (74)
P05	1.33	13.80 (25)	765	304 (5)	117	125	19.12 (44)
P05B	0.39	0.10 (2)	119	4.8 (4)	106	125	9.22 (6)
P05H	0.43	0.21 (1)	105	7.4 (7)	112	125	9.09 (5)
P2	1.34	13.74 (22)	698	303 (4)	135	146	6.82 (3)
P2B	0.30	0.00	78	0	116	145	2.47 (1)
P2H	0.28	0.21 (2)	101	3.5 (8)	117	146	3.72 (4)

did not change with the incorporation, which is already expected considering the hydromechanical stability of SBA-15.

The integrated areas of the (100), (110) and (200) peaks were calculated because these peaks have higher intensities and are more defined. The values (sum of the integrated areas of the peaks) are shown in the Table 6. Fig. 5(b) shows the SAXS results of the samples synthesized with TIPB/P123 = 0.5 mass ratio. In this case the (210) diffraction peak became apparent after the incorporation of the proteins. This fact is probably related to the reduction of contrast of electron density of smaller mesopores and micropores due to their filling. These smaller pores and micropores contribute significantly to the intensity of the scattering curve at high values of q [27]. Therefore, as the influence or the scattering due to them

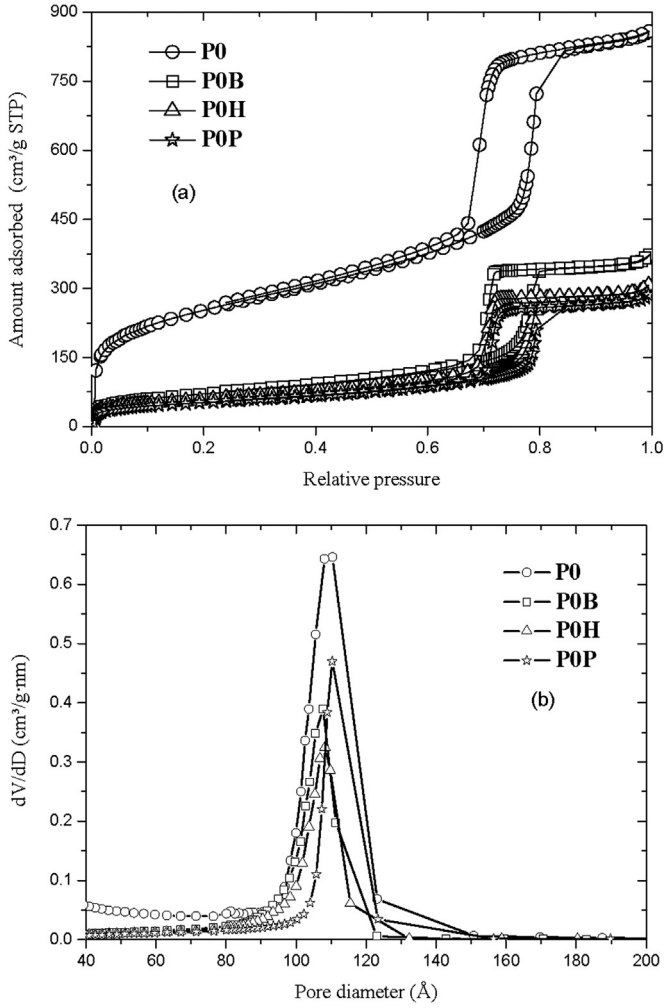

Fig. 6. (**a**) Isotherms and (**b**) pore size distribution of the conventional SBA-15 samples encapsulated with proteins and PBS.

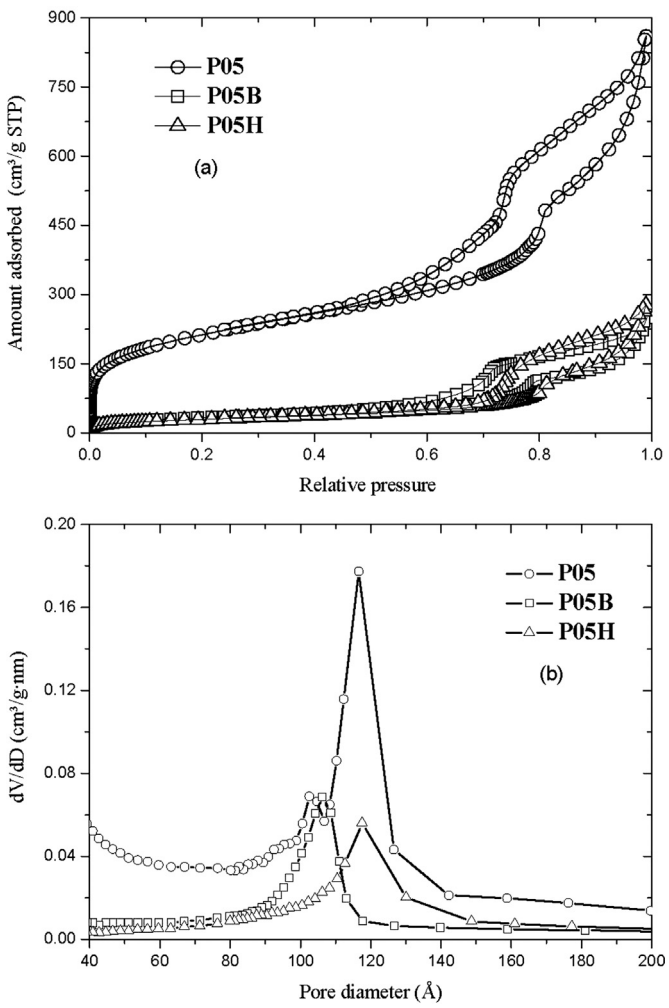

Fig. 7. (**a**) Isotherms and (**b**) pore size distributions of the SBA-15 samples with mass ratio TIPB/P123 = 0.5 encapsulated with proteins and PBS.

decreases, the scattering due to hexagonal network of mesopores becomes more evident causing the appearance of the (210) peak.

The NAI results are shown in Figs. 6–8. The reduction in volume and surface area of the micropores was larger than 95%. The micropores were filled only by PBS since the volume and specific surface area of micropores of this sample with only PBS, of the sample with BSA and of the sample with HGG are the same. In addition, the size of the proteins, which were approximately calculated in section 3.2, would not allow their encapsulation inside the micropores.

3.4. SAXS modeling

This section presents the parameters obtained with the theoretical model described in section 2.2. The fits were made only for the SBA-15 samples without TIPB since the samples with expanded pores have only three diffraction peaks with very small integrated intensities compared to the diffraction peaks of the conventional sample.

Some parameters were fixed because they became unstable during the fit, they are: $\nu = 0.01$, $\sigma_{int} = 3.0$, $L = 5000$ Å and $Rg = 50$ Å. The background parameter has two different values: for P0 sample $Sc_{const} = 1.4 \cdot 10^{-2}$ and to the others samples $Sc_{const} = 0.26 \cdot 10^{-2}$. The results are shown in Table 7 and Fig. 9.

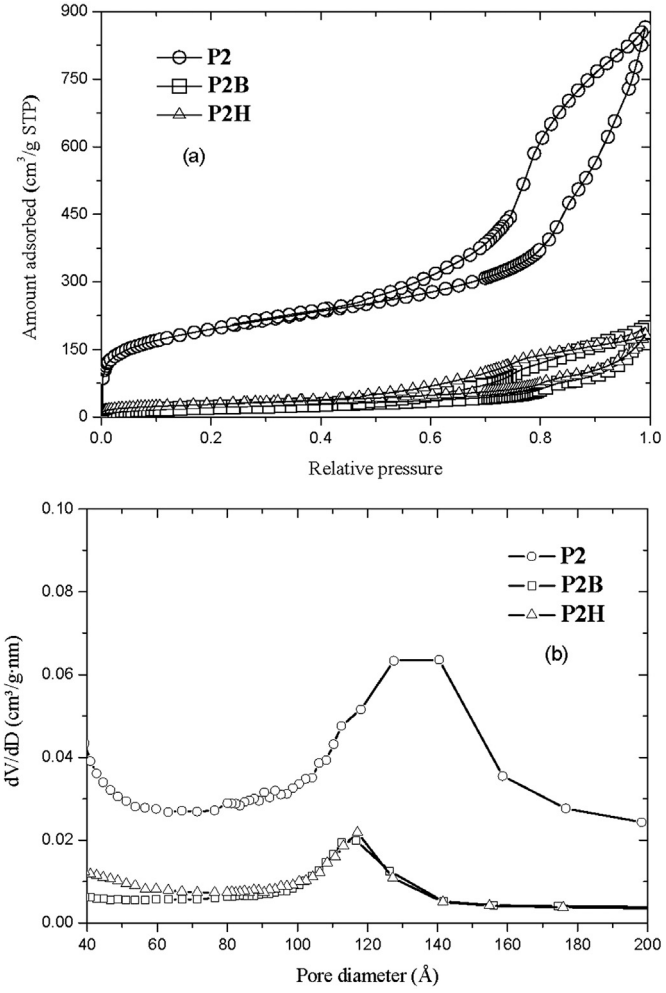

Fig. 8. (**a**) Isotherms and (**b**) pore size distributions of the SBA-15 samples with mass ratio TIPB/P123 = 2 encapsulated with proteins and PBS.

Table 7
Parameters obtained by fitting the SAXS data of the SBA-15 samples with proteins. The χ^2 is the reduced chi-squared and it is an estimative of the quality of the fit.

Parameter	P0	P0P	P0B	P0H
Sc_1	$0.53\ (6) \cdot 10^4$	$1.56\ (17) \cdot 10^4$	$5.71\ (14) \cdot 10^4$	$4.08\ (13) \cdot 10^4$
Sc_2	0.76 (20)	1.35 (7)	1.38 (13)	1.17 (12)
C	12.6 (5)	4.0 (4)	4.0 (2)	4.8 (2)
a (Å)	119 (1)	118 (1)	118 (1)	118 (1)
D (Å)	$8.85\ (69) \cdot 10^3$	$8.62\ (44) \cdot 10^3$	$8.62\ (44) \cdot 10^3$	$8.62\ (44) \cdot 10^3$
σ_a	$8.68\ (14) \cdot 10^{-2}$	$5.81\ (23) \cdot 10^{-2}$	$5.81\ (23) \cdot 10^{-2}$	$5.81\ (23) \cdot 10^{-2}$
R_{in} (Å)	54.3 (3)	49.0 (3)	50.0 (8)	51.1 (9)
R_{out} (Å)	64.3 (3)	75.2 (3)	75.4 (2)	74.6 (2)
$\Delta\rho_{out}/\Delta\rho_{in}$	11 (2)	1.42 (5)	1.10 (1)	1.08 (1)
σ_R/R	$11.4\ (2) \cdot 10^{-2}$	$7.5\ (3) \cdot 10^{-2}$	$7.6\ (1) \cdot 10^{-2}$	$7.9\ (1) \cdot 10^{-2}$
χ^2	4.1	5.2	9.1	7.9

4. Discussion

The SAXS results indicated that, on average, the pore network remained hexagonal with the TIPB addition. As expected, the PSD curve of the P0 sample presented a narrow distribution of pore sizes, while the samples synthesized with TIPB presented a broader distribution of pore diameters, which is characteristic of a more polydisperse pore network. The average pore diameter increased with the mass ratio TIPB/P123, the sample with the highest amount of TIPB has an average pore diameter 23% higher than the conventional sample P0. The volume and the micropore specific surface area did not change significantly with the expansion of the mesopores. The SAXS results showed that BSA has dimensions that allow its encapsulation inside the pores of the SBA-15 samples, as shown in section 3.1. The *p(r)* of the HGG shows a shapeless peak at $r \approx 70$ Å, which indicates, as in the BSA case, that the particles of the HGG have maximum diameter of 270 Å and the other two dimensions have an average value of $r \approx 70$ Å. Thus, the particles of the HGG sample also can be captured inside the pores of the SBA-15. The total areas of the SAXS peaks of the samples with proteins are smaller than the total areas of the peaks of the samples without protein. This is an indication of the presence of proteins and PBS inside the silica pores since the reduction of the scattering intensity of the diffraction peaks indicates a decrease in the electron density contrast between the pores and the silica matrix. There was no significant difference between the experimental results for samples with BSA and HGG, with the exception of the sample P2. The area of the diffraction peaks of the sample with PBS is higher than the areas of the diffraction peaks of samples with proteins, due to the fact that the sample with only PBS has a lower absorption than the other samples and also that part of the proteins could enter the mesopores. The micropore volume and surface area of the P2B sample have lower values than the accuracy of t-plot method, therefore these parameters were considered as zero (Table 6). The pore size distributions also indicated a filling of larger pores since the average pore diameter was shifted to lower values. This decrease is more evident for samples with expanded pores (Figs. 7(b) and 8(b)). The P0P sample presents a mean pore diameter slightly larger than the P0 sample without protein, again indicating the filling of pores of smaller diameters by PBS. Also, the BET specific surface area of this sample has a lower value than the values of the samples with BSA and HGG. These results indicate that the presence of the protein molecules may obstruct the pores and also interfere with the capacity of PBS molecules to adsorb on the silica pores. It is noticeable that the encapsulation of BSA is more effective than HGG due to its smaller size, being a result more evident for the P05 samples when compared to the P2 samples. The incorporation of proteins caused a decrease in the loop of the

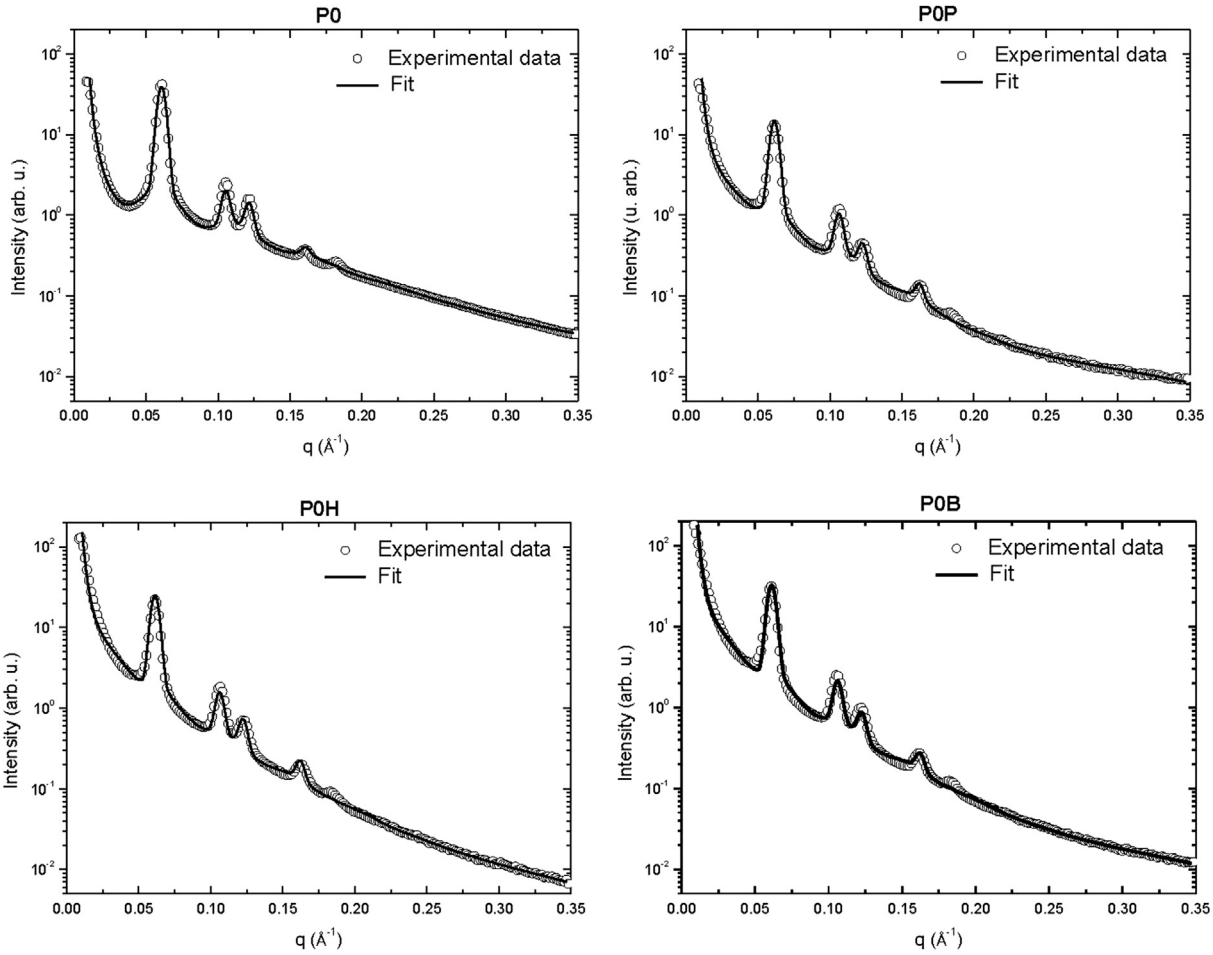

Fig. 9. SAXS data and fitting curves of the P0, P0B, P0H and P0P samples.

isotherms, as well as in the maximum adsorption amount. This fact is related to the decrease of the total volume and specific surface area of the pores. The filling of the total specific pore volume ranged from 60 to 80%, confirming the filling of the pores signaled by the SAXS measurements. The percentage variation in the total specific pore volume and BET specific surface area is higher for samples with expanded pores and increases with the increase of average pore diameter, initially suggesting that samples with larger average diameters and lattice parameters could lead to even larger variations in BET surface area and total pore volume.

Analyzing the results obtained from the SAXS model, it is important to notice that the scale factor Sc_1 presented an increase with the incorporation of PBS and proteins, indicating the formation of clusters that cause extra scattering. Comparing the sample with HGG and BSA one verifies that this extra scattering is larger for the sample with BSA. The modification of the parameter Sc_2 when compared to the values of the P0 sample, similar for the P0P, P0H and P0B samples, indicates the filling of the micropores by the PBS solution, in agreement with the results of section 3.3. The pore radius R_{in} decreased after the incorporation of PBS and it is not different for samples with proteins. This fact may be another evidence of the partial filling of the mesopores. The outer radius R_{out} increased after the addition of PBS and protein indicating an electronic density contrast difference between pores and silica walls after PBS incorporation in the micropores. The variation in the $\Delta\rho_{out}/\Delta\rho_{in}$ is different for samples with proteins when compared with the sample with only PBS, which indicates the presence of the proteins inside the pores of the material. The c parameter presented a similar decrease for the samples with PBS and proteins, so this change is related to the filling of pores by PBS. The variation in the σ_a disorder parameter is similar for the samples with PBS and proteins and less than the value of pure SBA-15.

5. Conclusions

In this paper we confirmed that the addition of TIPB provided silica with larger pores and with a more disordered pore network. The SAXS measurements indicated that the pore network remained, on average, hexagonal even after the addition of a large amount of TIPB. The increase in pore size and lattice parameter reached values of the order of 24% and 20%, respectively. This shows that, in order to obtain a larger pore diameter, changes in other synthesis parameters are required such as, for example, the synthesis temperature. The total specific pore volume remained unchanged with the TIPB addition. The increase of the average pore diameter is followed by a decrease in the BET specific surface area due to the cylindrical shape of the mesopores. It was possible to perform estimations of the size of the BSA and HGG proteins in order to verify if their dimensions are compatible with incorporation into the silica pores. The results indicated that the BSA and HGG proteins have dimensions compatible with their incorporation within the mesopores of SBA-15 samples. The measurements of the silica samples with proteins revealed that more than 95% of the micropores were filled by PBS. Although it has been shown that the

proteins could be incorporated inside the mesopores, a significant fraction of the proteins probably remained in the macroporosity of the material since there was no significant difference between the analyzed results of SAXS and NAI related to BSA and HGG encapsulation into the silica samples. These proteins may obstruct the mesopores entrance. The percentage of total pore volume, filled by the incorporation of the proteins, presented a small increase, following the increase of the average pore diameter. The larger diameter led to a better fit of the proteins and PBS molecules inside silica pores. The total pore volume decreased by 56 to 79% and a BET specific surface area by 72 til 89%. The micropores filling and the partial filling of the silica mesopores by the proteins were confirmed by the analysis made with a theoretical SAXS model.

Acknowledgments

This research is under the scope of the International Patents **WO07/030901**, **IN 248654**, **ZA 2008/02277**, **KR 1089400, MX 297263, HK 1124791, JP 5091863, CN 101287491B, CA 2621373, US 8642258 B2 and EP 1942934 B1.** Thanks are due to Fundação de Amparo à Pesquisa do Estado de São Paulo [FAPESP CeTICS Program 2013/07467-1], CNPq, Cristália Produtos Químicos Farmacêuticos Ltda. and UNIEMP Institute for the financial support. Márcia C. A. Fantini, Cristiano L.P. Oliveira and Osvaldo A. Sant'Anna are researchers of CNPq – Brazil.

Appendix A. Supplementary data

Supplementary data related to this article can be found at http://dx.doi.org/10.1016/j.micromeso.2016.07.033.

This work reports new experimental results about the synthesis process to prepare an ordered mesoporous silica matrix with large pores and its use as an efficient vehicle for encapsulation and release of different proteins. Future applications of SBA-15 with expanded pores as a vaccine adjuvant is an expansion of our pioneer work about oral immunization.

References

[1] A. Sayari, P. Liu, Non-silica periodic mesostructured materials: recent progress, Microporous Mater. 12 (Dec 1997) 149–177.
[2] C.T. Kresge, M.E. Leonowicz, W.J. Roth, J.C. Vartuli, J.S. Beck, A new family of mesoporous molecular sieves prepared with liquid crystal templates, Nature 359 (Oct 22 1992) 710–712.
[3] K.S.W. Sing, Reporting physisorption data for das solid systems – with special reference to the determination of surface-area and porosity, Pure Appl. Chem. 54 (1982) 2201–2218.
[4] T.J. Pinnavaia, S.A. Bagshaw, E. Prouzet, Templating of mesoporous molecular-sieves by nonionic polyethylene oxide surfactants, Science 269 (Sep 1 1995) 1242–1244.
[5] D.Y. Zhao, J.L. Feng, Q.S. Huo, N. Melosh, G.H. Fredrickson, B.F. Chmelka, et al., Triblock copolymer syntheses of mesoporous silica with periodic 50 to 300 angstrom pores, Science 279 (Jan 23 1998) 548–552.
[6] D. Zhao, Q. Huo, J. Feng, B.F. Chmelka, G.D. Stucky, Nonionic triblock and star diblock copolymer and oligomeric surfactant syntheses of highly ordered, hydrothermally stable, mesoporous silica structures (vol 120, pg 6024, 1998), J. Am. Chem. Soc. 136 (Jul 23 2014) 10546.
[7] J.S. Beck, J.C. Vartuli, W.J. Roth, M.E. Leonowicz, C.T. Kresge, K.D. Schmitt, et al., A new family of mesoporous molecular sieves prepared with liquid crystal templates, J. Am. Chem. Soc. 114 (Dec 30 1992) 10834–10843.
[8] R.M. Rioux, H. Song, J.D. Hoefelmeyer, P. Yang, G.A. Somorjai, High-surface-area catalyst design: synthesis, characterization, and reaction studies of platinum nanoparticles in mesoporous SBA-15 silica, J. Phys. Chem. B 109 (Feb 17 2005) 2192–2202.
[9] C.G. Wu, T. Bein, Conducting carbon wires in ordered, nanometer-sized channels, Science 266 (Nov 11 1994) 1013–1015.
[10] C.G. Wu, T. Bein, Conducting polyaniline filaments in a mesoporous channel host, Science 264 (Jun 17 1994) 1757–1759.
[11] D.I. Fried, D. Bednarski, M. Dreifke, F.J. Brieler, M. Thommes, M. Froba, Influence of the hydrophilic-hydrophobic contrast of porous surfaces on the enzymatic performance, J. Mater. Chem. B 3 (2015) 2341–2349.
[12] Z. Zhou, M. Hartmann, Progress in enzyme immobilization in ordered mesoporous materials and related applications, Chem. Soc. Rev. 42 (2013) 3894–3912.
[13] J. Meissner, A. Prause, C. Di Tommaso, B. Bharti, G.H. Findenegg, Protein immobilization in surface-functionalized SBA-15: predicting the uptake capacity from the pore structure, J. Phys. Chem. C 119 (Feb 5 2015) 2438–2446.
[14] C. Charnay, S. Begu, C. Tourne-Peteilh, L. Nicole, D.A. Lerner, J.M. Devoisselle, Inclusion of ibuprofen in mesoporous templated silica: drug loading and release property, Eur. J. Pharm. Biopharm. 57 (May 2004) 533–540.
[15] J.F. Diaz, K.J. Balkus, Enzyme immobilization in MCM-41 molecular sieve, J. Mol. Catal. B-Enzymatic 2 (Dec 4 1996) 115–126.
[16] L. Cao, T. Man, M. Kruk, Synthesis of ultra-large-pore SBA-15 silica with two-dimensional hexagonal structure using triisopropylbenzene As micelle expander, Chem. Mater. 21 (Mar 24 2009) 1144–1153.
[17] L.P. Mercuri, L.V. Carvalho, F.A. Lima, C. Quayle, M.C.A. Fantini, G.S. Tanaka, et al., Ordered mesoporous silica SBA-15: a new effective adjuvant to induce antibody response, Small 2 (Feb 2006) 254–256.
[18] L.V. Carvalho, R. d. C. Ruiz, K. Scaramuzzi, E.B. Marengo, J.R. Matos, D.V. Tambourgi, et al., Immunological parameters related to the adjuvant effect of the ordered mesoporous silica SBA-15, Vaccine 28 (Nov 23 2010) 7829–7836.
[19] F. Mariano-Neto, J.R. Matos, L.C. Cides da Silva, L.V. Carvalho, K. Scaramuzzi, O.A. Sant'Anna, et al., Physical properties of ordered mesoporous SBA-15 silica as immunological adjuvant, J. Phys. D-Applied Phys. 47 (Oct 22 2014).
[20] J.R. Matos, L.P. Mercuri, M. Kruk, M. Jaroniec, Toward the synthesis of extra-large-pore MCM-41 analogues, Chem. Mater. 13 (May 2001) 1726–1731.
[21] D.I. Svergun, L.A. Feigin, G.W. Taylor, Structure Analysis by Small-angle X-ray and Neutron Scattering, Springer, 1987.
[22] A.V. Semenyuk, D.I. Svergun, GNOM – a program package for small-angle scattering data-processing, Journal of Appl. Crystallogr. 24 (Oct 1 1991) 537–540.
[23] I. Pilz, O. Glatter, and O. Kratky, "Small-angle X-ray Scattering," ed.
[24] D. Svergun, C. Barberato, M.H.J. Koch, CRYSOL – a program to evaluate x-ray solution scattering of biological macromolecules from atomic coordinates, J. Appl. Crystallogr. 28 (Dec 1 1995) 768–773.
[25] P.V. Konarev, V.V. Volkov, A.V. Sokolova, M.H.J. Koch, D.I. Svergun, PRIMUS: a Windows PC-based system for small-angle scattering data analysis, J. Appl. Crystallogr. 36 (Oct 2003) 1277–1282.
[26] G.A. Zickler, S. Jaehnert, W. Wagermaier, S.S. Funari, G.H. Findenegg, O. Paris, Physisorbed films in periodic mesoporous silica studied by in situ synchrotron small-angle diffraction, Phys. Rev. B 73 (May 2006).
[27] S. Manet, J. Schmitt, M. Imperor-Clerc, V. Zholobenko, D. Durand, C.L.P. Oliveira, et al., Kinetics of the formation of 2D-Hexagonal silica nanostructured materials by nonionic block copolymer templating in solution, J. Phys. Chem. B 115 (Oct 6 2011) 11330–11344.
[28] A. Sundblom, C.L.P. Oliveira, A.E.C. Palmqvist, J.S. Pedersen, Modeling in situ small-angle x-ray scattering measurements following the formation of mesostructured silica, J. Phys. Chem. C 113 (May 7 2009) 7706–7713.
[29] P. Debye, Molecular-weight determination by light scattering, J. Phys. Chem. 51 (1947).
[30] M. Kotlarchyk, S.H. Chen, Analysis of small-angle neutron-scattering spectra from polydisperse interacting colloids, J. Chem. Phys. 79 (1983) 2461–2469.
[31] T. Neugebauer, Calculation of the light diffusion of filament chain solutions, Ann. Der Phys. 42 (1942) 509–533.
[32] J.S. Pedersen, D. Posselt, K. Mortensen, Analytical treatment of the resolution function for small-angle scattering, J. Appl. Crystallogr. 23 (Aug 1 1990) 321–333.
[33] S. Brunauer, P.H. Emmett, E. Teller, Adsorption of gases in multimolecular layers, J. Am. Chem. Soc. 60 (Jan-Jun 1938) 309–319.
[34] E.P. Barrett, L.G. Joyner, P.P. Halenda, The determination of pore volume and area distributions in porous substances .1. Computations from nitrogen isotherms, J. Am. Chem. Soc. 73 (1951) 373–380.
[35] M. Jaroniec, L.A. Solovyov, Improvement of the Kruk-Jaroniec-Sayari method for pore size analysis of ordered silicas with cylindrical mesopores, Langmuir 22 (Aug 1 2006) 6757–6760.
[36] B. Lippens, B. Linsen, J. De Boer, Studies on pore systems in catalysts I. The adsorption of nitrogen; apparatus and calculation, J. Catal. 3 (1964) 6.
[37] N. Freiberger, O. Glatter, Small-angle scattering from hexagonal liquid crystals, J. Phys. Chem. B 110 (Aug 3 2006) 14719–14727.
[38] P.V. Konarev, M.V. Petoukhov, D.I. Svergun, MASSHA – a graphics system for rigid-body modelling of macromolecular complexes against solution scattering data, J. Appl. Crystallogr. 34 (Aug 2001) 527–532.
[39] O. Glatter, O. Kratky, Small Angle X-ray Scattering, 102, Academic Press, London, 1982.
[40] E.O. Saphire, P. Parren, R. Pantophlet, M.B. Zwick, G.M. Morris, P.M. Rudd, et al., Crystal structure of a neutralizing human IgG against HIV-1: a template for vaccine design, Science 293 (Aug 10 2001) 1155–1159.